The Journal of Physiology

Electrolyte transport pathways induced in the midgut epithelium of *Drosophila melanogaster* larvae by commensal gut microbiota and pathogens

Shubha R. Shanbhag[1], Abraham T. Vazhappilly[1], Abhay Sane[1], Natalie M. D'Silva[1] and Subrata Tripathi[1,2]

[1] *Tata Institute of Fundamental Research, Colaba, Mumbai, 400 005, India*
[2] *Institute of Physics, Sachivalaya Marg, Bhubaneswar, 751 005, India*

Key points

- The digestive tract of larval and adult *Drosophila* is an excellent analogue of the mammalian gut. Enterocytes of the posterior midgut are separated by septa, with no paracellular path, and therefore perform both immune and transport functions.
- Using microperfusion electrophysiology, we show that larvae emerging from the embryo into sterile medium have symmetrical apical and basal membrane conductances while larvae emerging into non-sterile medium have apical membranes fivefold more conductive than basal membranes. The channels inserted into the apical membranes could originate in microbiata or host and mediate recognition of microbes.
- Entomopathogenic cyclic peptide toxins deplete intracellular ions reversibly, forming transient ion channels that do not conduct water, unlike an ionophore like nystatin that depletes ions irreversibly.
- We show the feasibility of studying the interaction of a single microbial species, or tractable combinatorials of microbial species, with only enterocytes in the primary epithelial barrier.

Abstract Microbiota colonizing exposed epithelial surfaces are vital for sustenance of metazoan life, but communication between microbiota, epithelial cells and the host immune system is only beginning to be understood. We address this issue in the posterior midgut epithelium of *Drosophila* larvae where nutrient transport and immune functions are exclusively transcellular. We showed that larvae emerging into a sterile post-embryonic environment have symmetrical apical and basal membranes. In contrast, larvae emerging into non-sterile media, the source of microbiota, have markedly asymmetrical membranes, with apical membrane conductance more than fivefold higher than the basal membrane. As an example of pathogen action, we showed that the entomopathogenic fungal toxin destruxin A (Dx) depleted intracellular ions. Reversibility of action of Dx was verified by bilayer reconstitution in forming transient non-specific channels that conduct ions but not water. Dx was also less effective from the apical side as compared to the basal side of the epithelium. We also showed that intercellular septa are not conductive in non-sterile cells, even though most cells are isopotential. Luminal microbiota therefore impart asymmetry to the epithelium, by activation of apical membrane conductance, enhancing inter-enterocyte communication, separated by insulating septa, via the gut lumen. These results also open the possibility of studying the basis of bidirectional molecular conversation specifically between enterocytes and microbiota that enables discrimination between commensals and pathogens, establishment of the former, and elimination of the latter.

(Received 14 April 2016; accepted after revision 20 June 2016; first published online 4 July 2016)
Corresponding author S. Tripathi: Institute of Physics, Sachivalaya Marg, Bhubaneswar 751 005, India. Email: tripathi@tifr.res.in or barakote@gmail.com

DOI: 10.1113/JP272617

Abbreviations Bf, bafilomycin A_1; BM, bilayer membrane; CS, canton S strain; DMSO, dimethyl sulfoxide; Dx, destruxin A; Gf, germ free; GMO, glycerol monooleate; Gr, gramicidin A; I_{sc}, short circuit current; ISM, ion selective microelectrode; Ny, nystatin; pH_i, intracellular pH; pH_o, extracellular pH; PTFE, polytetrafluoroethylene; R_a, apical membrane resistance; R_b, basal membrane resistance; R_t, transepithelial resistance; Sch-R, Schneider Ringer; V_a, apical membrane potential; V_b, basal membrane potential; V_c, transepithelial potential at collection end; V_h, holding potential; V_k, membrane potential with potassium exchanger; V_m, cell membrane potential; V_{Na}, membrane potential with sodium exchanger; V_{pH}, membrane potential with hydrogen exchanger; V_t, transepithelial potential at perfusion end.

Introduction

Species-specific microbiota bound to epithelial surfaces are absolute requirements for normal development and sustenance of metazoan life forms, from *Hydra* (Rahat & Dimentman, 1982) to mammals (Hooper & Gordon, 2001; Duerkop *et al.* 2012). Their absence from the intestine results in severe impairment of nutrition and development (Sekirov *et al.* 2010; Douglas, 2011; Erkosar *et al.* 2013; Broderick *et al.* 2014; Wong *et al.* 2015; Bonfini & Buchon, 2016), but our understanding of the molecular conversation between gut epithelial cells and microbiota in the lumen is rudimentary. In the mammalian intestine, where enterocytes are held together at tight junctions that allow permeation of small and large solutes and water (Naftalin & Tripathi, 1986) and even processes of dendritic or goblet cells, paracellular transfer of antigens and signalling molecules (Sekirov *et al.* 2010; Ashida *et al.* 2011; Shen *et al.* 2011; McDole *et al.* 2012) adds to the complexity of host–microbe interaction. Conversely, insect epithelia like the posterior midgut of *Drosophila* larvae are assembled by septa between homogeneous cells (Shanbhag & Tripathi, 2005, 2009; Banerjee *et al.* 2006) with no discernible paracellular path across the epithelium. Such epithelia perform transport and immune functions only transcellularly, interfaced with the apical membrane facing orally ingested microbiota in the lumen, and the basal membrane facing cul-de-sac respiratory tracheoles and sterile haemolymph (Shanbhag & Tripathi, 2005). This fortuitous, exclusively transcellular model of apical and basal membranes in series, permits focusing on the response of the epithelial cell only to luminal microbiota. The larval gut of *Drosophila* is a very powerful tight epithelium, generating pH gradients from 1 to 11 along its length and a high short-circuit current, and has other electrolyte transport pathways similar to the mammalian intestine, but a unique cellular homeostasis that requires special pharmacological tools to unravel (Shanbhag & Tripathi, 2005, 2009). Microperfusion of individual gut segments with a homogeneous cell population allows independent control of solutions bathing the luminal or basal membrane and unilateral drug application to test sidedness of action where necessary. In this study, we concentrate on the posterior segment of the midgut that is known to alkalinize the lumen, and is the best characterized segment from the ultrastructural and physiological viewpoints.

Early measurements of gut segments perfused *in vitro* indicated that the apical membrane was considerably more depolarized and highly conductive when compared to the basal membrane (Shanbhag & Tripathi, 2005), without any electron microscopic or other evidence of membrane damage. The luminal space adjacent to the apical membrane brush border of gut epithelia has a layer of material thought to be an immune barrier, a mucin layer in vertebrates (Ashida *et al.* 2011), or a chitin–glycoprotein peritrophic matrix in insects (Kuraishi *et al.* 2011; Weiss *et al.* 2014). Removal of the peritrophic membrane and *in vitro* perfusion (Shanbhag & Tripathi, 2005) permit direct access to, and assessment of, the intrinsic resilience of the apical membrane. Enterocytes not only face pathogen or toxin challenges from the gut lumen, but also potentially through the arborization of respiratory tracheoles, which terminate close to the basement membranes (Shanbhag & Tripathi, 2005, 2009). Consequently, the mechanism of adaptive immune responses in insect colonies (Konrad *et al.* 2012) would be determined at least partly by the susceptibility of apical and basal membranes to oral or respiratory access of pathogens. As both apical and basal membranes could underpin innate host defence mechanisms, we selected the entomopathogenic cyclic peptide toxin destruxin A (Dx), secreted by the fungus *Metarhizium anisopliae*, and the basal plasma membrane H^+-V-ATPase inhibitor bafilomycin A_1 (Bf) as probes to assess apical and basal membrane properties. The reported effects of Dx are diverse (Pal *et al.* 2007; Ruiz-Sanchez *et al.* 2010; 2012) and suggested mechanisms that trigger a cascade of intracellular effects are conflicting. It has even been suggested that Dx is not an ionophore or a V-ATPase inhibitor (Dumas *et al.* 1996). We therefore investigated the mechanism of action of Dx in more detail.

Little is also known of the early process of recovery from pathogen and toxin challenge (Charroux & Royet, 2012; Capo *et al.* 2016). Isolated gut studies from the basal side only provide little information on the apical membrane, which is the main interface with microbiota. Microperfusion solves this problem by providing controlled access to the lumen, where solution composition and other parameters can be controlled. Combined with ion-selective and conventional

Table 1. Composition of Ringer solutions

Component	Solution *a* (Control)	Solution *b* (*Schneider)	Solution *c* (Sucrose)
NaCl	130.0	87.0	—
$NaHCO_3$	10.0	6.7	10.0
NaH_2PO_4	0.5	0.3	—
Na_2HPO_4	0.1	0.07	—
$CaCl_2$	1.8	1.2	1.8
$MgCl_2$	1.0	0.7	1.0
DL-Alanine	0.5	0.3	0.5
D-Glucose	10.0	6.7	10.0
KCl	5.0	3.3	5.0
Sucrose	—	—	245
Schneider insect medium	—	+	—
Mean osmolarity (mosmol l^{-1})	286	287	288
Mean resistivity (Ω cm)	93	100	671

Solution *a*, control Ringer; solution *b*, Schneider Ringer; solution *c*, sucrose Ringer. Concentrations are in mM. The pH of perfusion–superfusion solutions *a* and *c* were titrated to 7.2 with either 1 M KOH or 1 M HCl. Solutions were bubbled with a 95% O_2–5% CO_2 gas mixture. Trypan blue dye was added to solution *a* in lumen to exclude cell damage at the beginning of each experiment, but was not present during physiological recording. *Schneider Ringer was made by dissolving 2.8 g of Schneider insect medium (Sigma-Aldrich) in 80 ml of distilled water and filtered using 0.22 μm filters; pH was adjusted to 7.2 with 1 M NaOH and the volume made up to 100 ml; to this 200 ml of solution *a* was added.

Table 2. Supplementation with Schneider medium prolongs viability with sustained and higher transepithelial transport

	Solution		V_t (mV)	R_t (Ω cm^2)	I_{sc} (μA cm^{-2})	V_b (mV)	V_a (mV)	R_a/R_b
A	L	Control-R	−43.6 ± 6.4	1189 ± 229	36.9 ± 9.0	−65.8 ± 6.7	22.2 ± 6.0	0.36 ± 0.11
	B	Control-R	($n = 11$)	($n = 8$)	($n = 8$)	($n = 11$)	($n = 11$)	($n = 8$)
	L	Control-R + 0.1% DMSO	−41.7 ± 5.4	1178 ± 260	35.4 ± 10.8	−70.6 ± 5.7	28.9 ± 5.7	0.42 ± 0.2
	B	Control-R + 0.1% DMSO	($P > 0.5$)	($P > 0.8$)	($P > 0.5$)	($P > 0.8$)	($P > 0.5$)	($P > 0.5$)
B	L	Sch-R	−46.9 ± 1.6	672 ± 43	65.8 ± 5.6	−64.8 ± 2.6	17.9 ± 2.3	0.44 ± 0.16
	B	Sch-R	($n = 44$)	($n = 44$)	($n = 44$)	($n = 44$)	($n = 44$)	($n = 44$)
	L	Sch-R	−46.0 ± 2.3	760 ± 40	57.4 ± 3.7	−70.3 ± 5.5	24.3 ± 6.2	0.65 ± 0.24
	B	Control-R	($P > 0.4$)	($P > 0.07$)	($P > 0.1$)	($P > 0.4$)	($P > 0.3$)	($P > 0.08$)

Values for perfused midgut, both ends cannulated and electrically sealed from bath. B, bath solution; L, lumen solution; Sch-R, Schneider Ringer. I_{sc}, short circuit current; R_a, apical membrane resistance; R_b, basal membrane resistance; R_t, transepithelial resistance; V_a, apical membrane potential; V_b, basal membrane potential; V_t, transepithelial potential at perfusion end.

microelectrodes, simultaneous data of both apical and basal membranes can be obtained. We were further able to control the microbial content of the lumen by germ-free (Gf) cultures of embryos to enable comparison of epithelial properties with normal symbiotic microbiota. Likewise, the effects of pathogens on gut epithelia were evaluated not by direct application of bacterial cultures to the epithelium, but by selective use of a single, highly purified, stable, and soluble toxin, Dx. Unknown or indeterminate concentrations of toxin were thus avoided. Preliminary communications of subsets of these data have been presented to the Physiological Society (Shanbhag *et al.* 2011) and at the European *Drosophila* Research Conference, Barcelona (Shanbhag *et al.* 2013).

Methods

Ethical approval

No ethical approval was required for *Drosophila* experiments.

Fly Stocks, food preparation and germ-free culture

Actively feeding third-instar wild-type larvae of *Drosophila melanogaster* (Canton S strains, CS) were raised at room temperature (22–25°C) on maize flour 8.3%, D-glucose 5%, sucrose 2.5%, yeast powder 2%, agar 1.5%, propionic acid 0.4%, *o*-phosphoric acid 0.06%, methylhydroxybenzoate 0.01%. The chemicals for rearing

flies were of A.R. grade, and obtained from SD Fine chemicals (Mumbai, India). Sterile food was autoclaved for 15 min, in glass vials and capped with sterile plastic caps. Control conventional, non-sterile diet was autoclaved and sterile until dispensed outside a flow hood. Collections of 12-h embryos were washed in a nylon filter mesh with sterile distilled water followed by dechorionation in ∼3% sodium hypochlorite (Merck, Mumbai, India) and rinsed in sterile distilled water. They were then washed twice in 70% ethanol and twice with sterile distilled water; these embryos were transferred in a laminar flow hood into sterile food vials (Sterile treatment). In controls, embryos were similarly dechorionated, washed outside the flow hood and transferred into food vials.

Chemicals and solutions for perfusion

All chemicals and reagents were obtained from Sigma-Aldrich/Fluka (St Louis, MO, USA). Compositions and osmolarities of the perfusion and superfusion solutions

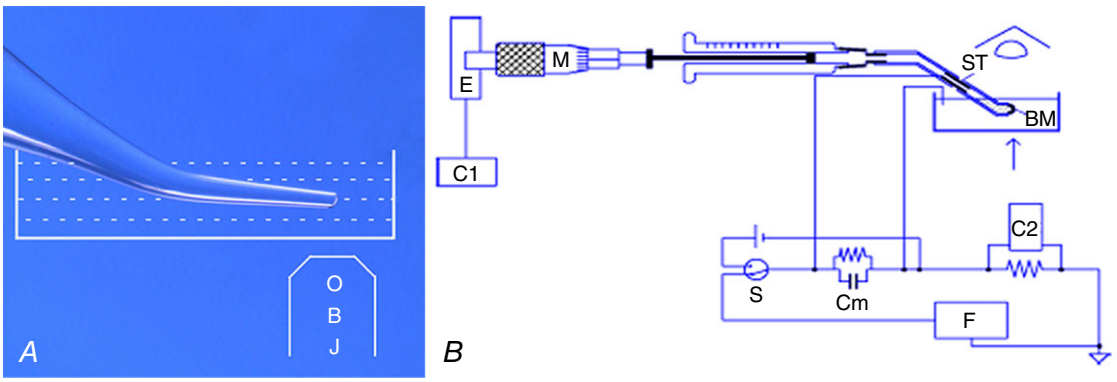

Figure 1. Ion conductance and water permeability of Dx channels reconstituted in bilayers
A, channel current recording: an aluminosilicate microelectrode (100 μm tip inner diameter) was bent on a microforge by 30 deg, silanized, filled with salt solution symmetrical with the bath, connected to a patch-clamp amplifier headstage and immersed in a grounded salt solution in a 35 mm Petri dish on the stage of an inverted microscope. A bilayer membrane (BM) was formed at the tip of the microelectrode. OBJ, Objective lens *B*, water flow measurement: a BM was formed at the tip of a bent polytetrafluoroethylene (PTFE) tube filled with and immersed in KCl solution in a plastic Petri dish grounded with an Ag/AgCl wire. The back of the PTFE tube was connected through an Ag/AgCl tube (ST) to a Hamilton syringe whose plunger was driven by a micrometer (M), connected to an absolute encoder (E). The Ag/AgCl pair was used to set the voltage across the bilayer at zero. Water flow across the bilayer was first driven by a gradient of 500 mM urea. The membrane was kept at a fixed position of an eyepiece graticule of a microscope so that the rate at which the syringe plunger had to be moved to keep the membrane position constant was the rate of water flow across the BM. Data were acquired through computers C1 for water flow and C2 for membrane capacitance. Cm, membrane circuit analogue; F, triangular function generator; S, make-before-break switch to toggle between voltage source and function generator.

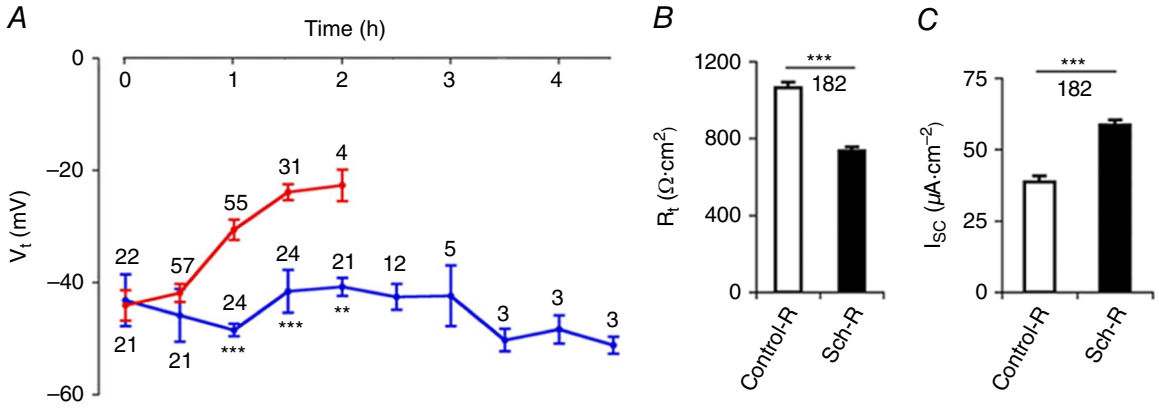

Figure 2. Prolonged midgut viability in Sch-R
A, gradual decay of transepithelial potential (V_t) with Control-R perfusion (Table 1 solution *a*, red trace) is reversed with Schneider supplementation (Sch-R, Table 1 solution *b*, blue trace); *B* and *C*, Sch-R supplementation also lowers transepithelial resistance (R_t; *B*) and increases short circuit current (I_{sc}; *C*). Number of experiments (n) is indicated in *A*–*C*. Graphs show mean ± SEM. $^{**}P < 0.01$, $^{***}P < 0.001$.

are given in Table 1. The pH of solutions was adjusted to 7.2 while stirring and bubbling with the 95% O_2–5% CO_2 gas mixture used during the experiment. Bafilomycin-A_1 (Bf) (Sigma-Aldrich, cat. no. B1793) or nystatin (Ny) (Sigma-Aldrich, cat. no. N6261) was dissolved in 0.1% dimethyl-sulfoxide (DMSO; Sigma-Aldrich, cat. no. D5879) diluted with either solution *a* or solution *b* (Table 1) to a final concentration of 10 μM and stored at –20°C until use. A stock solution of 500 μM destruxin A (Dx) (Sigma-Aldrich, cat. no. D4921) was prepared in DMSO as described before or in 1% ethanol (Sigma-Aldrich, cat. no. 32294). DMSO (0.1–1%, v/v)

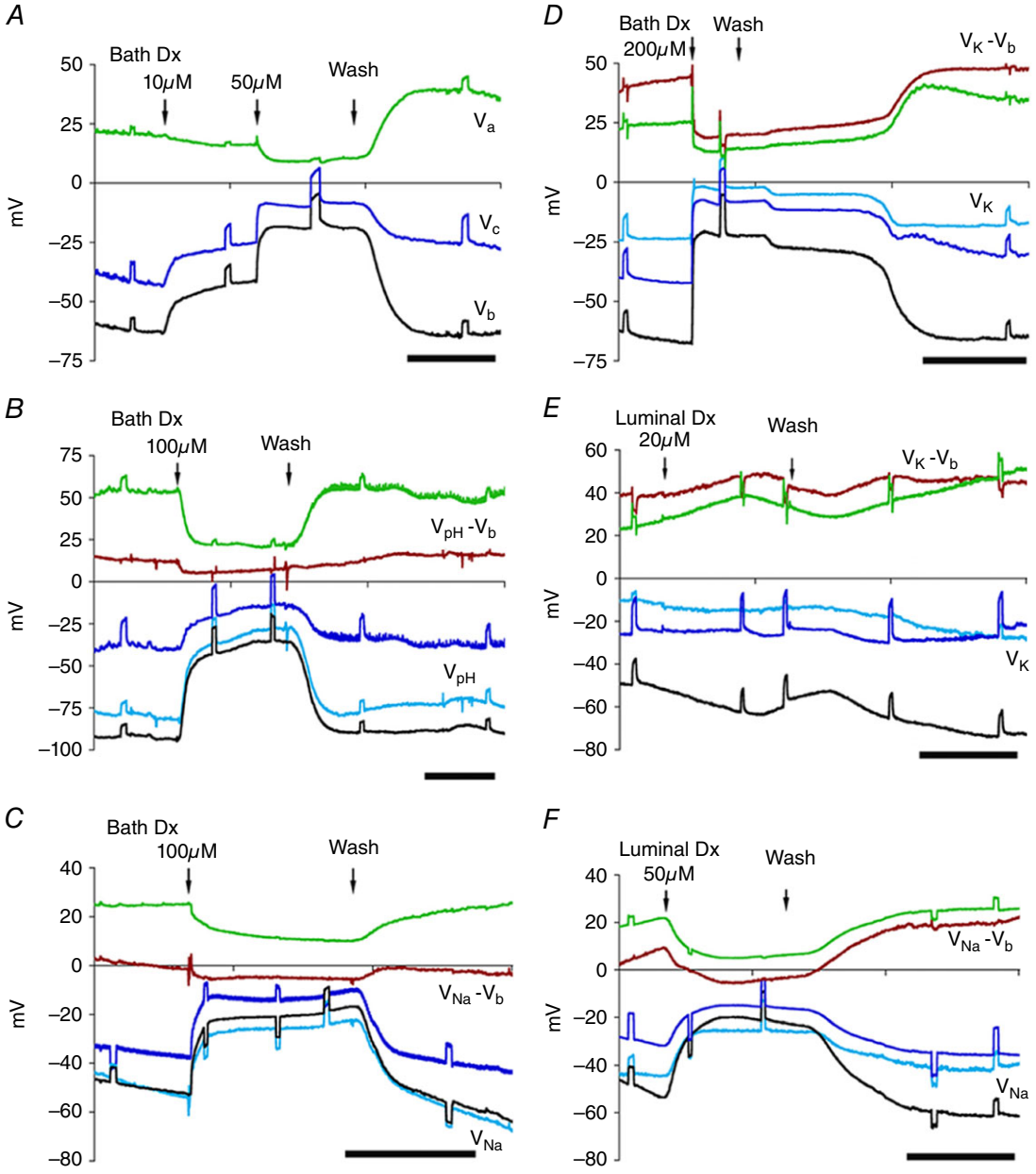

Figure 3. Dx is less effective from the apical side (representative electrical traces)
A–D, bath Dx: in Sch-R, V_c (blue trace), V_b (black trace), V_a (green trace) and intracellular ionic activities declined reversibly with graded doses of Dx. *A*, Dx 10 μM (threshold) depolarized V_c and V_b but not V_a; higher doses ($\geq$ 20 μM) depolarized V_a (cf. *A* and *D*) reversibly for concentrations $\leq$ 100 μM; after wash both V_a and V_b hyperpolarized. *B–D*, depletion of intracellular H^+ (*B*; see $V_{pH} - V_b$, brown trace), Na^+ (*C*; see $V_{Na} - V_b$ trace) and K^+ (*D*; see $V_K - V_b$ trace). *E*, luminal Dx of 20 μM has little effect; mild depolarization of the basal membrane V_b and very little decrease in $[K^+]_i$ (see $V_K - V_b$ trace) was observed with no change in V_c. *F*, luminal perfusion with 50 μM Dx depolarized V_t or V_c, V_b and V_a, and decreased $[Na^+]_i$ (see $V_{Na} - V_b$ trace). The short circuit current I_{sc} was reduced without affecting R_a/R_b ratio (see Fig. 4*E* and *F*). Scale bar, 5 min.

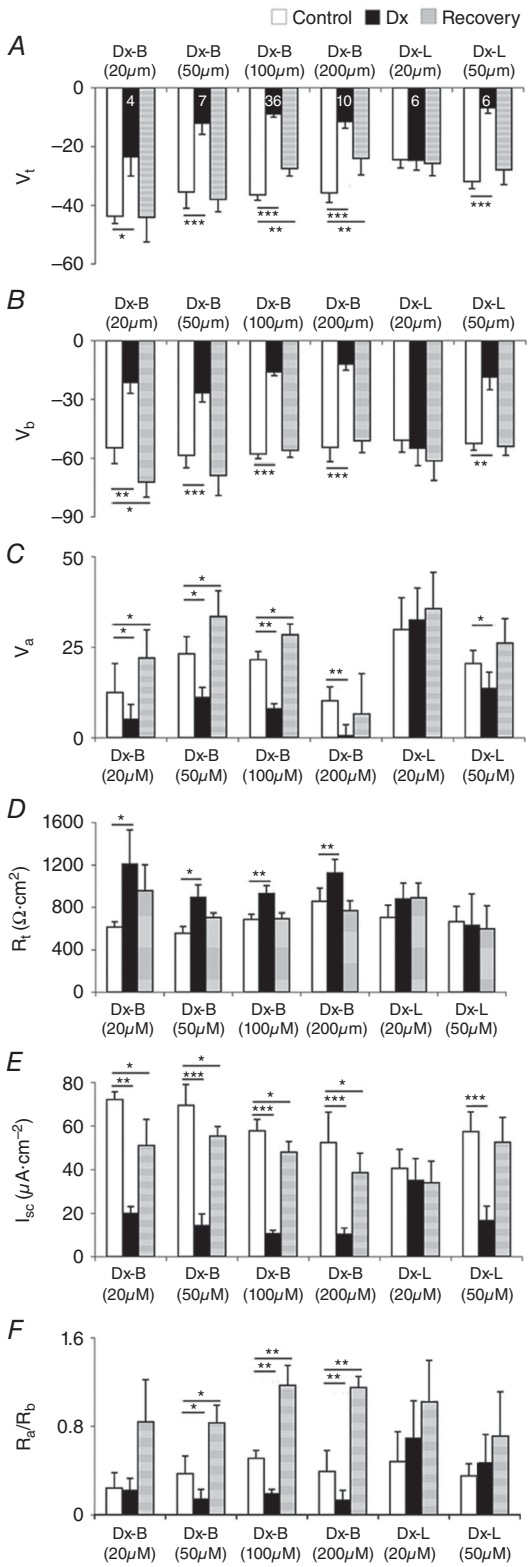

Figure 4. Dx is less effective from the apical side (pooled data)
Bath Dx 20–200 μM depolarized V_t (*A*), V_b (*B*) and V_a (*C*), increased R_t (*D*), and reduced I_{sc} (*E*) and R_a/R_b ratio (*F*). Luminal Dx at 20 μM is ineffective. Number of experiments (n) indicated in *A* is the same for *B–F*. Graphs show mean ± SEM. *$P < 0.05$, **$P < 0.01$, ***$P < 0.001$.

applied without toxins had no effect on transepithelial potentials (Table 2A). Perfusate concentrations of DMSO were ≤ 0.1% (v/v).

Microperfusion, transepithelial potential and resistance, and cell membrane resistance ratios

Posterior midguts of *Drosophila* larvae were initially microperfused and superfused with control solution of defined composition (Table 1, solution *a*) with coaxial glass capillaries as described earlier (Shanbhag & Tripathi, 2005). After stabilization of electrical parameters, the solutions were switched to have well-characterized Schneider Ringer (Sch-R) solutions (Table 1, solution *b*) bracketing each test manoeuvre. Transepithelial potentials (V_t and V_c) at perfusion and collection ends, respectively, of the gut were measured with Ringer-agar bridges and electrometers (models M-707 or 705; World Precision Instruments, Sarasota, FL, USA). Transepithelial resistance (R_t) was measured by terminated cable analysis (Shanbhag & Tripathi, 2005). The resistance ratio of apical and basal membranes (R_a/R_b) was calculated from the voltage deflections of an intracellular microelectrode in response to a 50–100 nA current pulse injected into the lumen with an electrometer (Duo 773 Electrometer, WPI) with the bath grounded.

Cell membrane potential and ion-selective microelectrode fabrication and calibration

Cell membrane potential (V_m) was measured from the basal side (V_b) using conventional microelectrodes (resistances of 20–60 MΩ when filled with 0.5 M KCl solution; tip potentials < 2 mV), pulled on a horizontal puller (Narishige, Tokyo, Japan, model PN-3), using 1.0 mm OD borosilicate capillaries (Omega dot, Frederick Haer, Bowdoin, ME, USA or from Sutter Instruments, Novato CA, USA, cat. no. BF-100-50-10). Apical membrane potential (V_a) was calculated as the difference between transepithelial potential at perfusion end (V_t) and basal membrane potential (V_b). To determine the extracellular and intracellular ionic activities, liquid-ion-exchanger microelectrodes were fabricated on a Sutter P-97 puller from acid-cleaned and dried aluminosilicate glass (Sutter cat. no. A150-100-10) and silanized as described by Tripathi *et al.* (1985) in a glass oven at 80°C in a fume hood. Ion-selective microelectrode (ISM) tip diameters were < 1 μm and the time constants for 90% response to solution changes were between 10 and 20 s. The pH-ISM tip was filled with H^+ ionophore I cocktail A (Fluka, cat. no. 95291), and back-filled with 0.1 M HCl solution. The tip of the Cl^- -ISM was filled with Cl^- ionophore I cocktail A (Fluka, cat. no. 24902) and back-filled with 0.5 M KCl; the K^+-ISM tip was filled with potassium ionophore I cocktail A (Fluka, cat. no. 60031)

and back-filled with 0.5 M KCl solution. Sodium ionophore I cocktail A (Fluka, cat. no. 71176) was used as the sensor in the Na^+-ISM and was back-filled with 0.25 M NaCl solution. Before calibration all ISMs were fitted with Ag/AgCl half-cells. ISM resistances were between 10 and 20 GΩ and were connected to high impedance HiZ-223 electrometers (Harvard Apparatus, Hamden, CT, USA).

ISMs for H^+ were calibrated in pH 4.01, 7.01 and 9.01 buffers and used if slopes between 55–62 mV per pH unit were measured ($n = 58$). The K^+-ISMs ($n = 55$) were calibrated in 1, 10 and 100 mM KCl solutions. The Cl^- -ISMs ($n = 28$), and Na^+-ISMs ($n = 32$) were calibrated in solution containing 2, 20 and 200 mM NaCl. Only electrodes showing a slope of 52–59 mV/decade change of K^+ or Na^+ concentration were used in the experiment. Selectivities between K^+-ISM and Na^+-ISM were measured using 1 M KCl and 1 M NaCl solutions. The mean selectivity ratio for the K^+-ISM was K^+:Na^+ ≥ 1:0.018 and for the Na^+-ISM was Na^+:K^+ ≥ 1:0.016. Activity coefficients for single electrolyte solutions were obtained from Robinson & Stokes (1970).

Electrophysiology, data acquisition and analysis

Simultaneous impalements of adjacent or neighbouring cells yield identical V_b values, indicating that the cells are electrically coupled. Therefore, intracellular ion activities were determined from the difference between the potentials of the ISM and the cell membrane potential (V_m) simultaneously inserted two or three cells apart. When precision positioning of microelectrode was required, a piezo-stepper (EXFO inchworm, model 8200, Montreal, Canada) was used. Unperfused midguts were stuck down on Petri dishes coated with poly-D-lysine (Sigma-Aldrich, cat. no. P6407) under standard control Ringer solution (solution *a*) and scanned as above with ISMs. All electrode signals were filtered at 30 Hz (low pass 4-pole Bessel) and acquired on a computer using a National Instruments (Austin, TX, USA) PCI-6110 data acquisition card and a BNC-2110 breakout box. Custom software using LabVIEW6i version 6.0.2 on Windows was used to display and record data directly on disc. At the end of each experiment, ISMs were recalibrated and data were included if there was no deviation of slope and selectivity of more than 3% from the start of the experiment.

Conductance of Dx reconstituted into planar lipid bilayers

Bilayers were formed at the tip (80–150 μm) of silanized aluminosilicate microelectrodes with the terminal 2 mm length made cylindrical and bent 30 deg on a micro-forge, and immersed in a Petri dish (Fig. 1*A*); this geometry facilitated clear visualization of the membrane with inverted optics. All plasticware and glass capillaries were used only once to avoid contamination between experiments. Membranes were formed from 1-mono-oleoyl-rac-glycerol (Sigma-Aldrich, cat. no.

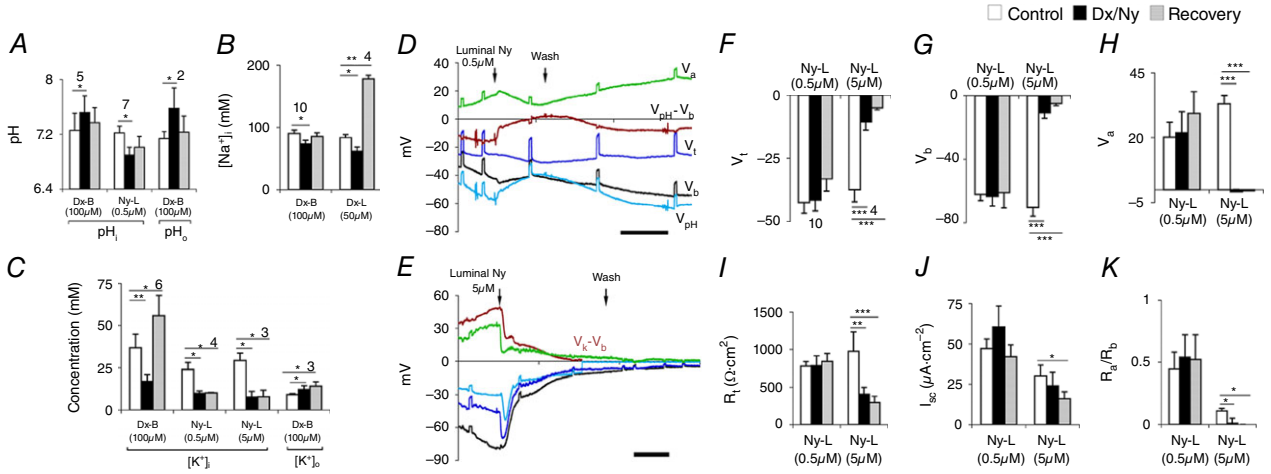

Figure 5. Irreversible depletion of electrolytes by Ny, but not by Dx
A, bath Dx increases both intracellular pH_i and extracellular pH_o reversibly, but luminal Ny acidifies pH_i. *B*, bath and luminal Dx decreases $[Na^+]_i$ reversibly with a rise after wash. *C*, with 100 μM bath or luminal Dx application, $[K^+]_i$ decreases and $[K^+]_o$ increases; also note sustained elevation of $[K^+]_i$ after recovery. Luminal Ny shows irreversible decrease in $[K^+]_i$. *D*, luminal Ny (0.5 μM) shows no change in V_t, V_b and V_a, but pH_i decreases (see $V_{pH} - V_b$, brown trace). *E*, perfusion of gut lumen with Ny (5.0 μM) depolarizes V_t, V_b and V_a and irreversibly reduces intracellular potassium concentration $[K^+]_i$ ($V_K - V_b$, brown trace). *F–K*, luminal Ny (0.5 μM) does not affect transepithelial transport parameters such as V_t (*F*), V_b (*G*), V_a (*H*), R_t (*I*), I_{sc} (*J*) and R_a/R_b ratio (*K*). But ≥ 5 μM Ny in the lumen, irreversibly depolarizes V_t, V_b and V_a, and decreases R_t and I_{sc}. R_a/R_b approaches 0 in *K*. Scale bar, 5 min. Number of experiments (*n*) is indicated in *A–C* and *n* value indicated in *F* also applies to *G–K*. Graphs show mean ± SEM. $^*P < 0.05$, $^{**}P < 0.01$, $^{***}P < 0.001$.

Table 3. Dx depletes intra- and extracellular ionic concentrations in the posterior midgut

	Solution		$[K^+]_i$ (mM)	$[K^+]_o$ (mM)	$[Na^+]_i$ (mM)	$[pH_i]$
A	L	Sch-R	45.2 ± 8.6	—	—	7.43 ± 0.05
	B	Sch-R	($n = 2$)			($n = 2$)
	L	Sch-R + 20 μM Dx	52.5 ± 10.4	—	—	8.04 ± 0.4
	B	Sch-R	($P > 0.4$)			($P > 0.05$)
	L	Sch-R (recovery)	56.7 ± 12.5	—	—	8.08 ± 0.4
	B	Sch-R	($P > 0.1$)			($P > 0.05$)
B	L	Sch-R	—	—	83.5 ± 5.0	—
	B	Sch-R			($n = 4$)	
	L	Sch-R + 50 μM Dx	—	—	62.0 ± 6.7	—
	B	Sch-R			($P < 0.05$)	
	L	Sch-R (recovery)	—	—	178.0 ± 5.7	—
	B	Sch-R			($P < 0.01$)	
C	L	Sch-R	36.7 ± 8.1	9.15 ± 0.6	90.2 ± 5.5	7.26 ± 0.25
	B	Sch-R	($n = 6$)	($n = 3$)	($n = 10$)	($n = 5$)
	L	Sch-R	16.97 ± 4.0	12.2 ± 2.2	73.6 ± 5.8	7.52 ± 0.24
	B	Sch-R + 100 μM Dx	($P < 0.01$)	($P < 0.05$)	($P < 0.05$)	($P < 0.05$)
	L	Sch-R (recovery)	55.7 ± 12.1	14.1 ± 2.6	85.6 ± 5.7	7.37 ± 0.22
	B	Sch-R	($P < 0.05$)	($P < 0.05$)	($P > 0.05$)	($P > 0.4$)

Values for perfused midgut, both ends cannulated and electrically sealed. B, bath solution; L, lumen solution.

M7765) 10 mM, dissolved in hexadecane (Fluka, cat. no. 52209). A few membranes were made with phosphatidyl choline (Avanti Polar Lipids, Alabaster, AL, USA, cat. no. 850375P) in decane (Fluka, cat. no. 30540). Dx dissolved in ethanol was added to the Petri dish to a final apparent concentration of 2 μM. Membrane currents and holding voltages were recorded with an EPC-7 (HEKA, Lambrecht/Pfalz, Germany) or Axopatch 200B amplifier and Digidata 1440A interface (Molecular Devices, Sunnyvale, CA, USA) and analysed using pCLAMP v.10.2 (Molecular Devices). Bilayer capacitance was measured by applying a 1 V s^{-1} voltage ramp across the bilayer (Molecular Devices, 2011) and membrane areas were calculated using a specific capacitance of 0.6 and 0.4 μF cm^{-2} for hexadecane and decane, respectively.

Water permeability of Dx reconstituted in planar bilayers

A bilayer membrane (BM) was formed at the tip of a polytetrafluoroethylene (PTFE) tube (Wang *et al.* 1995; Tripathi & Hladky, 1998) immersed in and filled with KCl solution (40–50 mM, 700 μl in the bath) (Fig. 1*B*). The PTFE tube, with an attached Ag/AgCl tube electrode (Goodfellow, Cambridge, UK, OD 1.1 mm) was connected to a Hamilton syringe (250 μl) whose plunger was driven by a micrometer attached to an absolute rotary encoder (US Digital, Vancouver, WA, USA) reading 2^{16} bits per turn for position sensing. An Ag/AgCl electrode served as the bath ground. The area of the bilayer was derived from measurement of membrane capacitance as above. The position of the BM could be reliably controlled by the syringe using the eyepiece graticule of a dissection microscope placed vertically above and orthogonal to the equatorial plane of the bilayer. Water flow across the bilayer results in a shift of the position of the bilayer on the graticule; this displacement was nulled on the graticule by driving the syringe and measuring the displacement with the encoder (E). The flow values were displayed as point-by-point derivatives, averaged over 30 and 60 s, the latter being used for the final analysis. Water flow across the bilayer was first generated by an osmotic gradient of 0.5 M urea. After recording steady state control flows driven by urea for at least 4 min, peptide Dx or gramicidin A (Gr), each dissolved in 1% ethanol stock solution, was added to detect changes in flow, if any, with respect to urea controls. Gr (2.5 μl of a 1 mM solution) was added to urea solution (700 μl of 0.5 M urea in 50 mM KCl) to give a final apparent concentration of 3.57 μM. For Dx, 20 μl of 1 mM Dx stock solution was added to urea solution giving a final apparent Dx concentration of 28.57 μM.

Conductance measurements through intercellular septa

To determine intercellular coupling (Boulpaep & Sackin, 1980), the lumen was perfused with control-R solution (Table 1, solution *a*) and bipolar rectangular current pulses

were injected into cells with one microelectrode and the change in potential in the neighbouring cell was measured with another microelectrode (both with IE-251 electrometers, Harvard Apparatus). The test pulses were then repeated with nominal electrolyte-free, sucrose-R solution (Table 1, solution *c*) perfusing the lumen. Ionic activities in and close to the cells were recorded with ISMs, connected to Hi-Z 223 electrometers (Harvard Apparatus).

Data analysis and statistics

Data are presented as arithmetic means ± standard error of the mean (SEM). Each *n* value represents a separate midgut segment dissected from a separate larva. For bilayer data, each *n* value represents a separate bilayer with symmetrical or asymmetrical solutions in which the complete data set was recorded without the bilayer breaking. Data were compared for statistical significance using Student's paired and unpaired two-tailed *t* test. Paired data generally entailed comparison of data on the same gut in control, test and recovery phases. Unpaired data were generally derived from guts from different populations, e.g. sterile or germ-free (Gf) versus non-sterile. *P*-values < 0.05 were considered to be statistically significant and the levels of significance are given in legends to figures. The absence of comparison bars denotes significance levels > 0.05.

Results

Enhancement of viability of *in vitro* midgut preparations

Studying the entire sequence of toxin action and recovery necessitated prolonging the viability of *in vitro* midgut preparations. We achieved prolonged stability and viability of microperfused preparations by enriching the perfusion and superfusion Ringer with Sch-R medium (Fig. 2). With

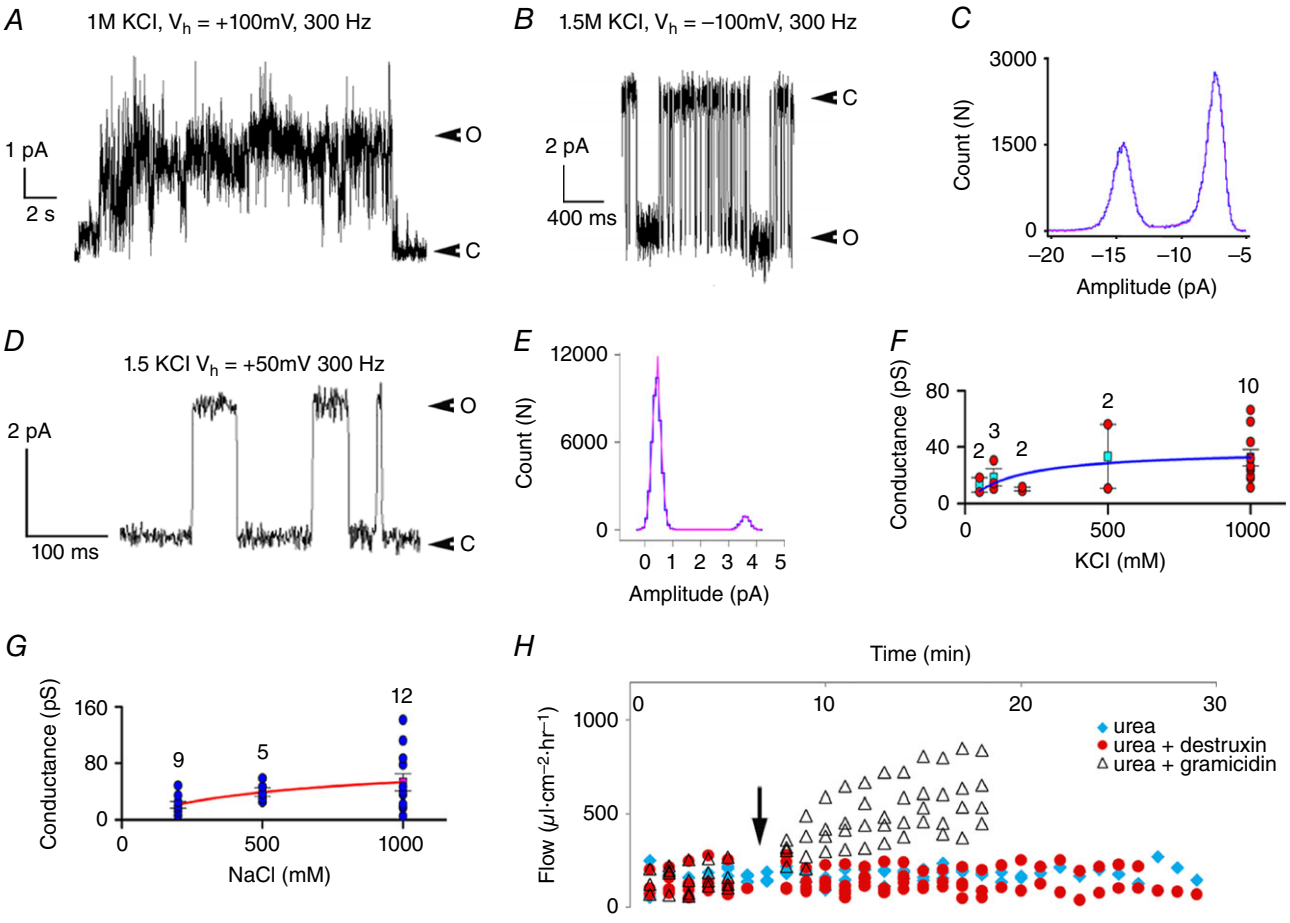

Figure 6. Reconstitution of Dx channels in bilayers for conductance and water flow measurements
A, sample current trace of Dx in a BM made from phosphatidyl choline prepared in decane (10 mM). *B*, sample current trace of Dx in a 10 mM glycerol monooleate (GMO)–hexadecane membrane. *C*, amplitude histogram of the current trace shown in *B*. *D*, Dx forms ion channels in GMO–hexadecane bilayers. O, open; C, closed. *E*, amplitude histogram and Gaussian fit of sample trace in *D*. Conductance in KCl in *F* (blue trace) and NaCl in *G* (red trace). Water flow driven across GMO–hexadecane bilayer by 500 mM urea (blue diamonds) is not increased by Dx (red circles) but increased by Gr (triangles) added at arrow. *n* value is indicated in *F*–*G*.

bilateral microperfusion of the midgut with Control-R (Table 1, solution *a*), V_t declined significantly (Fig. 2*A*, red trace). Supplementation of Ringer with Schneider medium (Sch-R, Table 1, solution *b*), particularly in the lumen, prevented the decline of transepithelial transport (Table 2B). Bilateral microperfusion with Sch-R enhanced V_t significantly (Control-R, –30.6 ± 1.8 mV *vs.* Sch-R, –48.5 ± 1.1 mV, after 30 min of perfusion; $P < 0.001$) as inferred from sustained V_t beyond 4 h (Fig. 2*A*, blue trace). Sch-R perfusion significantly lowered R_t (Control-R, 1064 ± 29 Ω cm^2 *vs.* Sch-R, 734 ± 21 Ω cm^2; $P < 0.001$, $n = 182$) (Fig. 2*B*), and R_a/R_b ratio (Control-R, 0.32 ± 0.02 *vs.* Sch-R, 0.19 ± 0.02; $P < 0.01$, $n = 100$). There was a significant increase in calculated I_{sc} (Control-R, 38.7 ± 2.0 μA cm^{-2} *vs.* Sch-R, 60.6 ± 2.8 μA cm^{-2}; $P < 0.001$, $n = 182$) (Fig. 2*C*). However no significant change in V_a and V_b was detected for Sch-R perfusion compared to control-R (Control-R, 19.4 ± 1.3 mV *vs.* Sch-R, 16.2 ± 1.9 mV and –60.6 ± 1.3 mV *vs.* –57.8 ± 1.6 mV, respectively; $P > 0.05$, $n = 117$).

Dx is less effective from apical side

Dx applied from the basal side rapidly depolarized apical, basal and transepithelial potentials (V_a, V_b, V_c/V_t, respectively) (Figs 3*A–D* and 4*A–C*), and depleted intracellular ions (Figs 3*B–D* and 5*A–C*, and Table 3). Effective (20 μM) concentrations of Dx dissolved in Sch-R and applied from the basal side, significantly and reversibly lowered V_t (control, –43.7 ± 2.5 mV *vs.* Dx, –23.5 ± 6.5 mV; $P < 0.02$, $n = 4$) (Fig. 4*A*), I_{sc} (control, 72.0 ± 3.6 μA cm^{-2} *vs.* Dx, 20.0 ± 3.0 μA cm^{-2}; $P < 0.01$, $n = 4$) (Fig. 4*E*) and increased R_t (control, 615 ± 51 Ω cm^2 *vs.* Dx, 1208 ± 323 Ω cm^2; $P < 0.05$, $n = 4$) (Fig. 4*D*). Up to Dx concentrations of 50 μM, significant depolarization of V_a (control, 23.2 ± 4.7 mV *vs.* Dx, 11.1 ± 2.8 mV; $P < 0.05$, $n = 7$) (Fig. 4*C*) and V_b (control, –58.6 ± 6.3 mV *vs.* Dx, –26.8 ± 4.7 mV; $P < 0.001$, $n = 7$) (Fig. 4*B*) was observed; following wash, a transient hyperpolarization of both V_a (control before Dx, 23.2 ± 4.7 mV *vs.* control after Dx, 33.5 ± 7.1 mV; $P < 0.03$, $n = 7$) (Figs 3*A*, green trace, and 4*C*) and V_b (control before Dx, –58.6 ± 6.3 mV *vs.* control after Dx, –68.9 ± 10.2 mV; $P > 0.4$, $n = 7$) (Figs 3*A*, black trace, and 4*B*) was also observed. From the luminal side, Dx (20 μM) was subthreshold (Figs 3*E* and 4*A–E*), and was effective only at doses above 50 μM (Figs 3*F* and 4*A–E*). Dx effects were surprisingly associated with an early and sustained, but reversible increase in R_t (Fig. 4*D*) and significant drop in R_a/R_b ratio (Fig. 4*F*) in a dose-dependent manner. Dose-dependent depletion of the major intracellular cations, H^+, Na^+ and K^+ (Figs 3*B–D*, *F* and 5*A–C*, and Table 3, A-C), while occurring as a consequence of a possible ionophore effect of Dx, needed reconciliation with elevated R_t. Indeed, the observed deflections in V_a and V_b due to constant-current pulses injected into the lumen (Fig. 3) indicate altered resistances of the two membranes with Dx. In order to unequivocally determine the mechanism of Dx action, we reconstituted Dx in artificial lipid BMs made from synthetic lipids.

Dx channels conduct ions but not water

To resolve the above paradoxical effects of Dx, we tested the effects of a well-characterized ionophore, Ny,

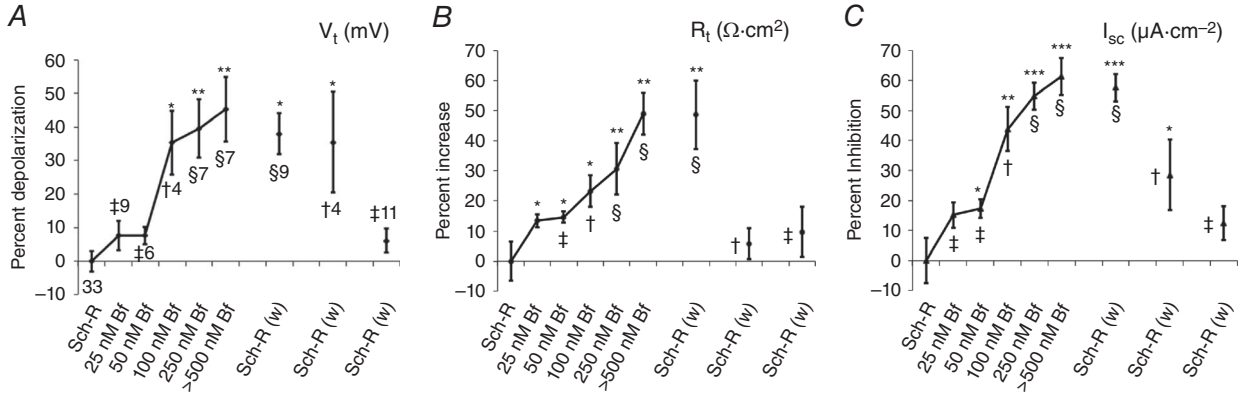

Figure 7. Inhibitory responses of Bf on enterocytes are greatly enhanced with Sch-R
A–C, plots of percentage depolarization for V_t in *A*, percentage increase for R_t in *B* and percentage inhibition for I_{sc} in *C* with increasing concentrations of Bf in Sch-R (Table 1, solution *b*) applied to the posterior midgut segment from the basal side shows a threshold inhibitory response at 100 nM Bf (labelled †) that is partially reversible (cf. Sch-R wash (w) marked †). Increasing concentration of Bf in the perfusate increases inhibition significantly. Doses of Bf ≥ 250 mM exhibit pronounced irreversible inhibition that appears to saturate with Bf > 500 nM (cf. Bf and Sch-R (w) labelled §). With doses of Bf < 100 nM, this inhibitory effect is completely reversible (cf. Bf and Sch-R (w) labelled ‡). Number of experiments *n* are indicated in *A* and are same for *B* and *C*. Plots show mean ± SEM. *$P < 0.05$, **$P < 0.01$, ***$P < 0.001$.

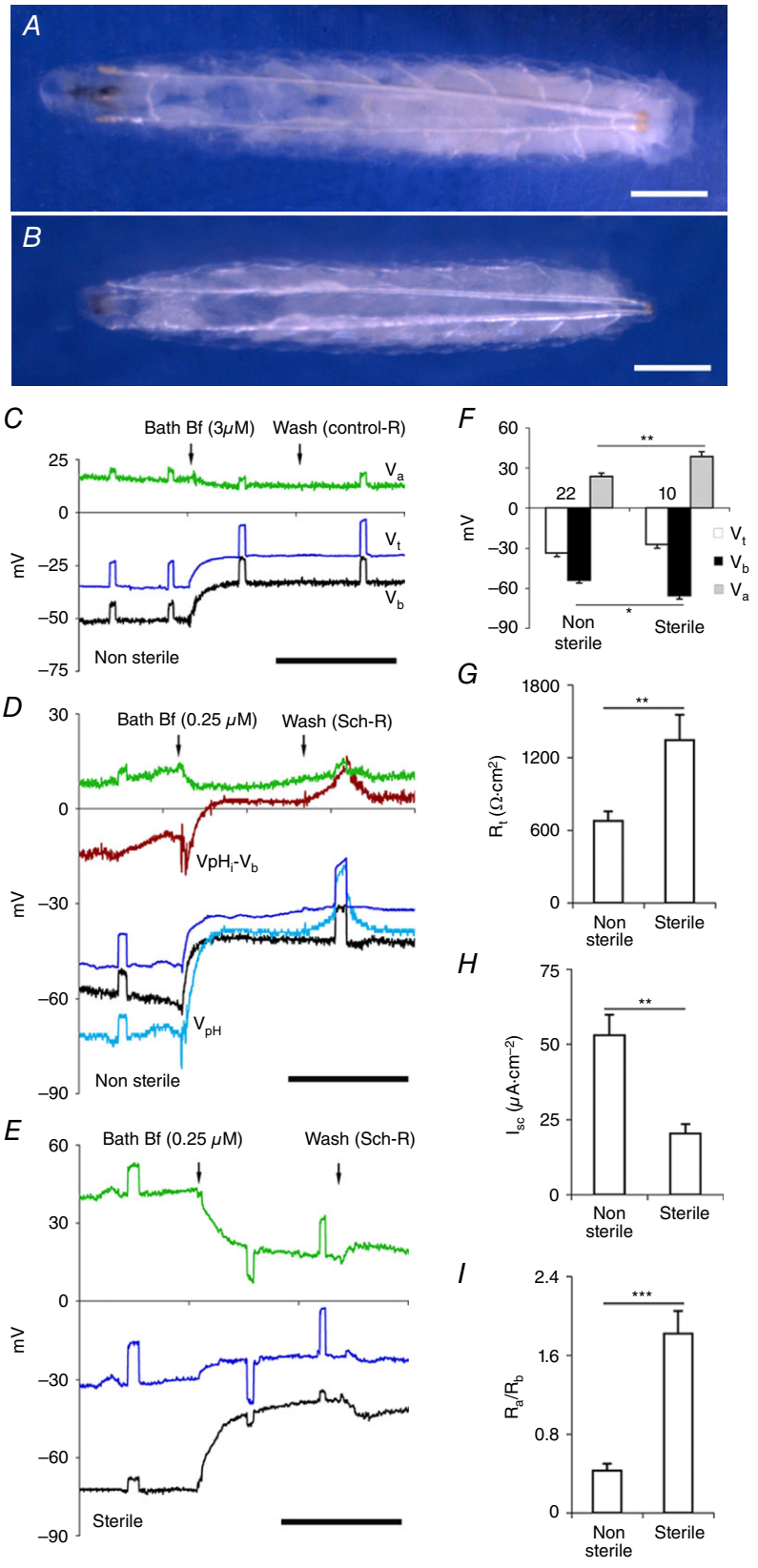

Figure 8. Sterile midguts have highly resistive apical membranes
A, an actively feeding *Drosophila* CS larva (approximately 109 ± 3 h from egg laying) emerging into non-sterile medium. *B*, *Drosophila* CS larvae of similar stage emerging into sterile medium show marginal reduction in size and attain this stage a day later than normal larvae (Non-sterile, 109 ± 3 h *vs.* Gf, 129 ± 5 h; 25°C; $n = 5$ experiments). Scale bar, 0.25 mm. *C–E*, basal application of Bf in all panels. Scale bar, 5 min. *C*, in posterior midgut segment of wild-type CS non-sterile strains, with perfusion with control-R (Table 1, solution *a*) V_b depolarized much more than V_a. *D*, perfusion with Sch-R (Table 1, solution *b*), apart from the elevated depolarization effect of V_c, V_b but not V_a, the intracellular H^+ increased and pH_i acidified (see $V_{pH} - V_b$, brown trace). *E*, sterile wild-type CS posterior midgut with Bf; V_a (green trace) and V_b (black trace) depolarizations are comparable. *F*, apical potential *Va* and basal potential *Vb* of sterile larvae were hyperpolarized. *G–I*, sterile larvae have increased R_t (*G*), decreased I_{sc} (*H*), and fivefold higher R_a/R_b ratio (*I*). Number of experiments (*n*) is shown in *F*, with transport parameters of each data set aligned vertically in *F–I*. Graphs show mean ± SEM. $^*P < 0.05$, $^{**}P < 0.01$, $^{***}P < 0.001$.

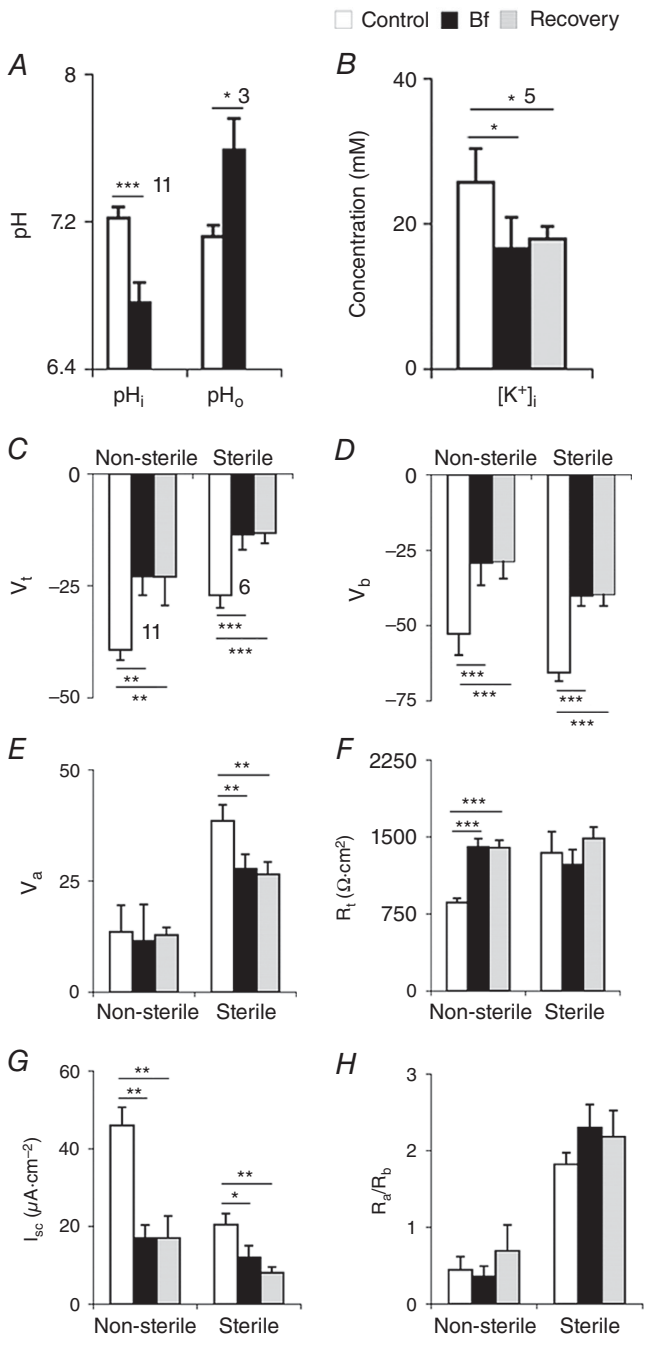

Figure 9. Sterile midguts have highly resistive apical membranes (pooled data)
A–B, bath application of Bf on posterior midguts of non-sterile larvae. *A*, Bf inhibited extrusion of H^+, resulting in acidification of cells and pH_o alkalinized. *B*, Bf decreased $[K^+]_i$ in the enterocytes. *C–H*, pooled data of all Bf (250 nM Bf in Sch-R) applications in non-sterile and sterile larval midguts. Sterile larvae have decreased V_t (*C*), V_b (*D*), V_a (*E*), I_{sc} (*F*) and increased R_t (*G*), with fivefold higher R_a/R_b ratio (*H*). Number of experiments (*n*) is indicated in *A* and *B* and *n* shown in *C* also applies to *D–H*. Graphs show mean ± SEM. $^*P < 0.05$, $^{**}P < 0.01$, $^{***}P < 0.001$.

which is known to permeabilize artificial and natural cell membranes to ions and water and dissipate ion gradients (Holz & Finkelstein, 1970), and compared its actions with those of Dx (Fig. 5). Luminal microperfusion with ≤ 0.5 μM Ny did not affect the transepithelial transport (Fig. 5*D* and *F–K*) but lowered the pH_i reversibly (control, 7.22 ± 0.1 *vs.* Ny, 6.9 ± 0.11; $P < 0.02$, $n = 7$) (Fig. 5*A* and *D*) and irreversibly decreased $[K^+]_i$ (control, 23.93 ± 4.1 mM *vs.* Ny, 9.86 ± 1.4 mM; $P < 0.05$, $n = 4$) (Fig. 5*C*). Nevertheless, luminal Ny ≥ 5.0 μM decreased transepithelial transport of the posterior midgut epithelial cells irreversibly (Fig. 5*E*). It depolarized V_t (control, –37.3 ± 4.8 mV *vs.* Ny, –10.6 ± 3.3 mV; $P < 0.001$, $n = 4$) (Fig. 5*F*), V_b (control, –70.4 ± 5.4 mV *vs.* Ny, –10.9 ± 3.5 mV; $P < 0.001$, $n = 4$) (Fig. 5*G*), and V_a (control, 33.1 ± 3.1 mV *vs.* Ny, –0.5 ± 0.9 mV; $P < 0.001$, $n = 4$) (Fig. 5*H*). R_t fell (control, 975 ± 258 Ω cm^2 *vs.* Ny, 409 ± 89 Ω cm^2; $P < 0.01$, $n = 4$) and further dropped to 298 ± 81 Ω cm^2 (Fig. 5*I*) and did not recover even after prolonged washing with Sch-R. Similarly, the R_a/R_b ratio also declined very rapidly (control, 0.11 ± 0.02 *vs.* Ny, 0.01 ± 0.04; $P < 0.05$, $n = 4$) and reached to near zero value during recovery (Fig. 5*K*). However, the apparent decrease in I_{sc} was not significant (control, 29.5 ± 6.9 μA cm^{-2} *vs.* Ny, 24.0 ± 8.5 μA cm^{-2}; $P > 0.05$, $n = 4$) (Fig. 5*J*). As expected, the higher dose of luminal Ny (5 μM) irreversibly decreased $[K^+]_i$ (control, 29.2 ± 4.4 mM *vs.* Ny, 7.6 ± 3.4 mM; $P < 0.05$, $n = 3$) (Fig. 5*C*).

As the Ny results did not unambiguously clarify the primary mechanism of actions of Dx, we reconstituted Dx into artificial lipid bilayer membranes at the tips of modified microelectrodes (Fig. 1*A*) and observed discrete conductances that were non-selective, spread over a large range (Fig. 6*A–G*), indicative of clustering of Dx, like other cyclic peptides (Fernandez-Lopez *et al.* 2001; Taira *et al.* 2010), and independent of the lipid charge (Fig. 6*B–D*). In contrast to linear helical peptides like Gr (Tripathi & Hladky, 1998), Dx did not increase the water permeability of the membrane (Fig. 6*H*).

Sterile midguts have highly resistive apical membranes

Membrane and transepithelial potential changes produced by endogenous currents provide accurate information about the distributed barriers of an epithelium (Boulpaep & Sackin, 1980), particularly if paracellular shunts are small. As the viability and transport in midgut preparations were greatly enhanced with Sch-R perfusion (Fig. 2*A*), we investigated the effects of Bf in Sch-R (Figs 7–9) and obtained a dose–response curve for V_t, R_t and I_{sc} (Fig. 7). At a threshold concentration of 50 nM Bf, V_t depolarized (7.6 ± 2.6%; $P < 0.08$, $n = 6$, Fig. 7*A*); R_t increased (14.6 ± 1.8%; $P \leq 0.04$, $n = 6$, Fig. 7*B*) and I_{sc} decreased (17.3 ± 3.1%; $P < 0.02$, $n = 6$, Fig 7*C*). Effects at

Table 4. Extracellular ion concentrations adjacent to the posterior midgut

Ion	Fly Strain Non-sterile (2nd instar)	Non-sterile (3rd instar)	Sterile (3rd instar)
$[K^+]_o$ (mM)	12.4 ± 1.3 ($n = 8$)	20.4 ± 2.5 ($n = 19$) ($P < 0.01$)	10.3 ± 0.4 ($n = 5$) ($P < 0.001$)
$[Cl^-]_o$ (mM)	165.0 ± 6.3 ($n = 9$)	180.5 ± 7.2 ($n = 11$) ($P > 0.1$)	141.2 ± 8.7 ($n = 8$) ($P < 0.01$)

Table 5. Membrane potential depolarization (mV) of posterior midgut enterocytes with Bf

Depolarization		Solution	Fly strain Non-sterile	Sterile
$\|\Delta V_b\|$	L	Sch-R	21.2 ± 3.6	21.1 ± 3.2
	B	Sch-R + 250 μM Bf	($n = 7$)	($n = 7$)
$\|\Delta V_a\|$	L	Sch-R	3.9 ± 1.5	18.6 ± 2.9
	B	Sch-R + 250 μM Bf	($P < 0.01$)	($P > 0.1$)

B, bath solution; L, lumen solution.

50 nM Bf were completely reversible (Fig. 7*A–C*, cf. marked ‡), at 100 nM partially reversible (Fig. 7*A–C*, labelled †), beyond which effects were completely irreversible despite prolonged washing (Fig. 7*A–C*, marked §). With Sch-R used as diluent, the Bf effects were 10-fold more pronounced in Sch-R as compared to Control-R (cf. Fig. 8*C* and *D*).

Larvae grown under sterile conditions are typically developmentally delayed (Chandler *et al.* 2011; Charroux & Royet, 2012). Therefore, to systematically compare the effects of gut microbiota, we grew larvae under non-sterile and sterile conditions at 25°C. To normalize larval sizes for purposes of comparison, actively feeding larvae in non-sterile media were selected at ∼109 ± 3 h from egg laying (Fig. 8*A*) and larvae growing in sterile media at ∼129 ± 5 h of egg laying (Fig. 8*B*). In sterile larvae, R_t is elevated (non-sterile, 679 ± 78 Ω cm^2, $n = 22$; *vs.* sterile, 1343 ± 210 Ω cm^2; $P < 0.01$, $n = 10$) (Fig. 8*G*) and I_{sc} is reduced (non-sterile, 53 ± 6.8 μA cm^{-2}, $n = 22$; *vs.* sterile, 20.4 ± 3.1 μA cm^{-2}; $P < 0.01$, $n = 10$) (Fig. 8*H*). Furthermore, V_a (non-sterile, 23.6 ± 2.4 mV, $n = 22$; *vs.* sterile, 38.5 ± 3.6 mV; $P < 0.01$, $n = 10$) (Fig. 8*F*, grey bar) and V_b (non-sterile, –53.9 ± 2.1 mV, $n = 22$; *vs.* sterile, –65.6 ± 2.8 mV; $P < 0.05$, $n = 10$) (Fig. 8*F*, black bar) are significantly hyperpolarized but V_t is unaltered (non-sterile, –33.5 ± 2.7 mV, $n = 22$; *vs.* sterile, –27.1 ± 2.8 mV; $P > 0.2$, $n = 10$) (Fig. 8*F* white bar).

In non-sterile larvae, Bf inhibits H^+ (Figs 8*D* and 9*A*) and also K^+ transport (Fig. 9*B*); pH_i decreased significantly (control, 7.22 ± 0.06 *vs.* Bf, 6.76 ± 0.11; $P < 0.001$, $n = 11$, Fig. 9*A*) and $[K^+]_i$ decreased irreversibly (control, 25.7 ± 4.7 mM *vs.* Bf, 16.6 ± 4.3 mM; $P < 0.05$, $n = 5$, Fig. 9*B*). Basal application of 2–3 μM Bf using Control-R or 0.25 μM Bf with Sch-R as diluent, depolarized V_t (Control-R, –41.6 ± 2.8 mV *vs.* Bf, –27.2 ± 2.3 mV; $P < 0.001$, $n = 21$; Sch-R, –39.3 ± 2.3 mV *vs.* Bf, –22.9 ± 4.2 mV; $P < 0.01$, $n = 11$) (Figs 8*C–D*, blue trace, and 9*C*), V_b (Control-R, –55.1 ± 3.3 mV *vs.* Bf, –36.7 ± 4.5 mV; $P < 0.001$, $n = 21$; Sch-R, –52.8 ± 7.5 mV *vs.* Bf, –29.2 ± 7.5 mV; $P < 0.001$, $n = 11$) (Figs 8*C–D*, black trace, and 9*D*), but did not affect V_a (Control-R, 13.6 ± 2.6 mV *vs.* Bf, 12.4 ± 2.4 mV; $P > 0.2$, $n = 21$; Sch-R, 13.5 ± 6.0 mV *vs.* Bf, 11.4 ± 8.3 mV; $P > 0.5$, $n = 11$) (Figs 8*C–D*, green trace, 9*E*). Bf significantly increased R_t (Control-R, 948 ± 234 Ω cm^2 *vs.* Bf, 1162 ± 242 Ω cm^2; $P < 0.001$, $n = 9$; Sch-R, 863 ± 39 Ω cm^2 *vs.* Bf, 1401 ± 82 Ω cm^2; $P < 0.001$, $n = 11$) (Fig. 9*F*) and decreased I_{sc} (Control-R, 47.5 ± 6.6 μA cm^{-2} *vs.* Bf, 24.6 ± 4.3 μA cm^{-2}; $P < 0.001$; $n = 9$; Sch-R, 46.0 ± 4.6 μA cm^{-2} *vs.* Bf, 17.0 ± 3.3 μA cm^{-2}; $P < 0.01$, $n = 11$) (Fig. 9*G*), but did not affect R_a/R_b ratio (Control-R, 0.47 ± 0.12 *vs.* Bf, 0.49 ± 0.1; $P > 0.5$, $n = 27$; Sch-R, 0.44 ± 0.15 *vs.* Bf, 0.36 ± 0.13; $P > 0.5$, $n = 11$) (Fig. 9*H*). In unperfused midgut preparations, extracellular scans showed reduced KCl absorption in sterile larvae as compared to non-sterile controls (Table 4).

Depolarization of V_a by Bf in non-sterile larvae was much less than V_b (Figs 8*C–D*, green and black

traces, and 9*D–E*). In contrast in sterile larvae, with basal application of Bf, V_a depolarization (Sch-R, 38.5 ± 3.6 mV *vs.* Bf, 27.7 ± 3.3 mV; $P < 0.01$, $n = 6$) was comparable to V_b depolarization (Sch-R, –65.6 ± 2.8 mV *vs.* Bf, –40.1 ± 3.4 mV; $P < 0.001$, $n = 6$) (Figs 8*E* and 9*D–E*), confirming that in the absence of microbiota, post-embryonic enterocytes remain near symmetrical with respect to circulating electrogenic currents (Table 5). The resistive properties of the apical membrane, particularly the resistance ratios of the apical and basal membranes (R_a/R_b) can also be inferred by external current injection into the lumen. This independently confirmed that the ratio of apical and basal membrane resistances remained fivefold higher in sterile larvae (non-sterile, 0.43 ± 0.07, $n = 22$; *vs.* sterile, 1.82 ± 0.23; $P < 0.001$, $n = 10$) (Figs 8*I* and 9*H*, and Table 5).

Conductance through intercellular septa is negligible

The larval midgut is known to be a tight epithelium with no discernible paracellular path (Shanbhag & Tripathi, 2005, 2009). However, the role of intercellular communication through the septa, in the plane of the epithelium, is not certain. As pathogens and toxins could propagate through this route, we assessed the electrical coupling between adjacent cells without *a priori* assuming gap junctions or cytoskeletal elements bridging the septate junctions (Banerjee, *et al.* 2006). By placing a single microelectrode each in two adjacent midgut epithelial cells (Fig. 10*A*, V_{b1} grey trace and V_{b2} black trace), we injected current into one cell to assess its spread to its neighbour. With Control-R (Table 1 solution *a*) flowing in the lumen, injection of a 50–80 nA current pulse into the lumen displaced both membrane potentials comparably (ΔV_{b1}, 2.96 ± 0.4 mV *vs.* ΔV_{b2}, 2.93 ± 0.6 mV, $P > 0.5$; $n = 7$) (Fig. 10*A*, inset 1 star, and *B*). However, the same current injected into cell through microelectrode V_{b1} (Fig. 10*A*, inset 1 grey trace, arrowhead) produced negligible displacement in V_{b2} (Fig. 10*A*, inset 1 black trace, arrowhead). Perfusing the lumen with insulating sucrose-R (Table 1, solution *c*) and injection of even higher currents directly into the lumen or into the cell via V_{b1} evoked negligible depolarization in the neighbouring cell (sucrose-R, 0.74 ± 0.1 mV *vs.* Control-R, 0.83 ± 0.1 mV, $P > 0.5$; $n = 5$) (Fig. 10*A*, inset 2 arrowheads, and *B*). Luminal current injection after the restoration of Control-R in the gut lumen restored the depolarization potentials in two neighbouring cells equally (V_{b1}, 2.64 ± 0.4 mV *vs.* V_{b2}, 2.53 ± 0.6 mV, $P > 0.5$; $n = 5$) (Fig. 10*A*, inset 3 star, and *B*). We also examined midguts before, during and after luminal sucrose-R perfusion to confirm viability. Luminal sucrose-R perfusion significantly depolarized V_t (control, –22.0 ± 1.4 mV *vs.* sucrose-R, 37.7 ± 13.5 mV, $P < 0.01$; $n = 5$),

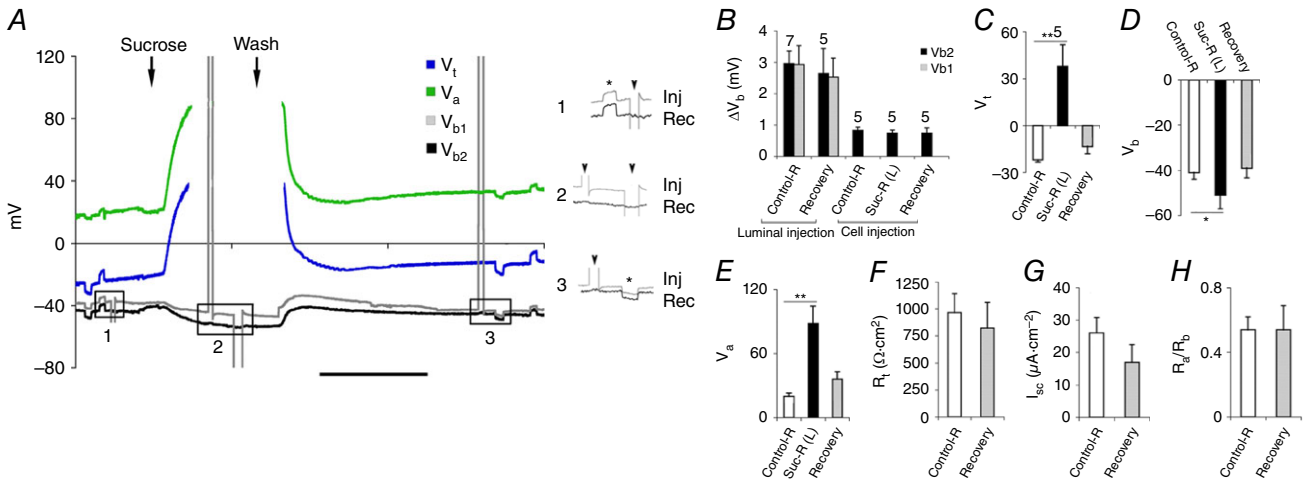

Figure 10. Conductance through intercellular septa is negligible
A, two microelectrodes inside adjacent cells record V_b (grey and black). Constant current pulses (~50 nA) injected into the lumen flowing Control-R (Table 1, solution *a*) depolarized both potentials (V_{b1} and V_{b2}) equally (inset 1, asterisk). The same current injected into one cell (inset 1, arrowhead for V_{b1}) did not affect V_{b2}. Even with perfusion of insulating sucrose-R (Table 1, solution *c*) in the lumen (inset 2), biphasic current pulses injected into V_{b1} (inset 2, arrowheads) were not detected by V_{b2}. Luminal current injection after restoration of Control-R in lumen restores V_{b1} and V_{b2} deflections (inset 3, asterisk). Scale bar, 5 min. *B*, 80 nA current injected into the lumen before and after insulating Ringer (Table 1, solution *c*) in the lumen produced identical displacement (ΔV_b) in V_{b1} and V_{b2}; the same current injected into one cell evoked negligible potential shifts in its neighbouring cell before, during and after luminal sucrose perfusion ($n = 5$ indicated in the figure). *C–E*, luminal sucrose-R reversibly depolarized V_t as shown in *C* and reversibly hyperpolarized V_b and V_a shown in *D* and *E* respectively. *F–H*, luminal sucrose-R did not affect R_t (*F*), I_{sc} (*G*) and R_a/R_b ratio (*H*). Graphs show mean ± SEM. $^*P < 0.05$, $^{**}P < 0.01$. Scale bar, 5 min. Number of experiments (*n*) shown in *C* applies also to *D–H*.

(Fig. 10*C*), hyperpolarized V_b (control, –40.9 ± 2.9 mV *vs.* sucrose-R, –50.5 ± 6.0 mV, $P < 0.05$, $n = 5$) (Fig. 10*D*) and V_a (control, 20.0 ± 3.0 mV *vs.* sucrose-R, 88.2 ± 16.5 mV, $P < 0.01$; $n = 5$) (Fig. 10*E*). These effects returned to normal after the restoration of luminal flow with Control-R (Fig. 10*C–E*). Sucrose-R perfusion did not affect R_t, I_{sc} or R_a/R_b ratios (Fig. 10*F-H*). These data demonstrate that gap junctions or connexin-like coupling does not occur between the posterior midgut enterocytes.

Discussion

We have shown that Dx begins its action as a pore-forming toxin, depleting ions, depolarizing enterocytes and inhibiting transport. Among multiple effects that follow, the increase in R_t taken together with the decrease in R_a/R_b ratio points to possible basal membrane channel inactivation. The recovery from toxin action leads to higher than basal transport rates, consistent with cellular responses that conserve energy and promote survival, e.g. oil-droplet formation, and inhibition of protein synthesis (Gonzalez *et al.* 2011). The separation of ions and water transport through cyclic peptides is a novel finding that implies cell volume changes after Dx action would be lower than with linear peptides allowing water permeation. The reversibility of Dx action could be due to a lower affinity of Dx for membrane components (Gonzalez *et al.* 2011) and may explain why Dx effects are reversible, even after high doses, but Ny effects are not. Intracellular depletion of H^+, Na^+ and K^+ (Figs 3*B–D*, *F* and 5*A–C*, and Table 3) due to Dx channel insertion into apical and basal membranes does not exclude the possibility of inactivation of other channels, possibly in the basal membranes, as a consequence. Indeed, the observed deflections in V_a and V_b due to constant-current pulses injected into the lumen (Fig. 3) indicate altered resistances of the two membranes with Dx. For this reason, with graded doses of Dx, we often observed a dissociation of V_t and V_b from V_a and R_{te} as the secondary rise in basal membrane resistance with Dx was considerable.

The absence of any conductive pathway through the intercellular septa and obvious cytoskeletal connectivity through the lateral membranes of the epithelium indicates that pathogens are unlikely to spread from cell to cell laterally, although spread through tracheoles, muscle and haemolymph can still occur (Apidianakis & Rahame, 2011; Panayidou & Apidianakis, 2013). The small decline in active transport rates after sucrose perfusion (Fig. 10*C–G*) is possibly related to adverse effects of Na^+ removal reported earlier (Shanbhag & Tripathi, 2009), but the passive properties were unaffected by the luminal manoeuvre.

The lipid and peptide composition of the apical membrane is clearly influenced by microbiota and needs further study to fully understand the relative ineffectiveness of Dx and Bf from the luminal side. Exposure of insects to sublytic doses of fungal toxins like Dx (Konrad *et al.* 2012) may act differently on either membrane and may be more effective through the respiratory rather than the oral route.

We have demonstrated the feasibility of retaining the postembryonic apical membrane in its native state before exposure to microbiota and studying its properties for several hours *in vitro*. This perfused preparation offers the opportunity of studying the effects of one or a combination of microbial species (Ryu *et al.* 2008; Sekirov *et al*, 2010; Wong *et al.* 2014; Douglas, 2015; Erkosar *et al.* 2015), or their soluble products, on both passive and active transport properties of the epithelium, and also intracellular changes consequent to pathogen challenge and recovery (Gonzalez *et al.* 2011; Limmer *et al.* 2011; Bofini & Buchon, 2016). The perfused *Drosophila* gut, with a structurally well-defined single layer of host epithelial cells with a high transport capacity in both larval and adult forms (Shanbhag & Tripathi, 2005, 2009), and a limited and defined set of microbiota (Ryu *et al.* 2008; Apidianakis & Rahame, 2011; Douglas, 2011; Gonzalez *et al.* 2011; Limmer, *et al.* 2011; Charroux & Royet, 2012), can also be used to evaluate the process of regeneration and repair (Micchelli & Perrimon, 2006; Ohlstein & Spradling, 2006) in the adult insect. The exact microbial species populating laboratory specimens as commensals is likely to be different from those in ambient settings (Chandler *et al.* 2011); the same is likely to be true of pathogens. Detailed analysis of the interaction of these species is possible, but beyond the scope of this study, in which we have concentrated on establishing feasibility.

References

Apidianakis Y & Rahme LG (2011). *Drosophila melanogaster* as a model for human intestinal infection and pathology. *Dis Model Mech* **4**, 21–30.

Ashida H, Ogawa M, Kim M, Mimuro H & Sasakawa C (2011). Bacteria and host interactions in the gut epithelial barrier. *Nature Chem Biol* **8**, 36–45.

Banerjee S, Sousa AD & Bhat MA (2006). Organization and function of septate junctions: an evolutionary perspective. *Cell Biochem Biophys* **46**, 65–77.

Bonfini A, Liu X, & Buchon N (2016). From pathogens to microbiota: How *Drosophila* intestinal stem cells react to gut microbes. *Dev Comp Immunol* **64**, 22–38.

Boulpaep EL & Sackin H (1980). Electrical analysis of intraepithelial barriers. In: *Current Topics in Membranes and Transport*, vol. **13**, ed. Bronner, F & Kleinzeller A, pp. 169–197. Academic Press, New York.

Broderick NA, Buchon N & Lemaitre B (2014). Microbiota-induced changes in *Drosophila melanogaster* host gene expression and gut morphology. *MBio* **5**, 1–13.

Capo F, Charroux B & Royet J (2016). Bacteria sensing mechanisms in *Drosophila* gut: local and systemic consequences. *Dev Comp Immunol* **64**, 11–21.

Chandler JA, Lang JM, Bhatnagar S, Eisen JA & Kopp A (2011). Bacterial communities of diverse *Drosophila* species: ecological context of a host-microbe model system. *PLoS Genet* **7**, e1002272.

Charroux B & Royet J (2012). Gut-microbiota interactions in non-mammals: What can we learn from *Drosophila*. *Semin Immunol* **24**, 17–24.

Douglas AE (2011). Lessons from studying insect symbioses. *Cell Host Microbe* **10**, 359–367.

Douglas AE (2015). Multiorganismal insects: diversity and function of resident microorganisms. *Annu Rev Entomol* **60**, 17–34.

Duerkop BA, Clements CV, Rollins D, Rodrigues JLM & Hooper LV (2012). A composite bacteriophage alters colonization by an intestinal commensal bacterium. *Proc Natl Acad Sci USA* **109**, 17621–17626.

Dumas C, Ravallec M, Matha V & Vey A (1996). Comparative study of the cytological aspects of the mode of action of destruxins and other peptidic fungal metabolites on target epithelial cells. *J Invertebr Pathol* **67**, 137–146.

Erkosar B, Storelli G, Defaye A & Leulier F (2013). Host-intestinal microbiota mutualism: learning on the fly. *Cell Host Microbe* **13**, 8–14.

Erkosar B, Storelli G, Mitchell M, Bozonnet L, Bozonnet N & Leulier F (2015). Pathogen virulence impedes mutualist-mediated enhancement of host juvenile growth via inhibition of protein digestion. *Cell Host Microbe* **18**, 445–455.

Fernandez-Lopez S, Kim H-S, Choi EC, Delgado M, Granja JR, Khasanov A, Kraehenbuehl K, Long G, Weinberger DA, Wilcoxen KM & Ghadiri MR (2001). Antibacterial agents based on the cyclic D,L-α-peptide architecture. *Nature* **412**, 452–455.

Gonzalez MR, Bischofberger M, Frêche B, Ho S, Parton RG & Goot FG (2011). Pore-forming toxins induce multiple cellular responses promoting survival. *Cell Microbiol* **13**, 1026–1043.

Holz R & Finkelstein A (1970). The water and nonelectrolyte permeability induced in thin lipid membranes by the polyene antibiotics nystatin and amphotericin B. *J Gen Physiol* **56**, 125–145.

Hooper LV & Gordon JI (2001). Commensal host-bacterial relationships in the gut. *Science* **292**, 1115–1118.

Konrad M, Vyleta ML, Theis FJ, Stock M, Tragust S, Klatt M, Drescher V, Marr C, Ugelvig LV & Cremer S (2012). Social transfer of pathogenic fungus promotes active immunization in ant colonies. *PLoS Biol* **10**, e1001300.

Kuraishi T, Binggeli O, Opota O, Buchon N & Lemaitre B (2011). Genetic evidence for a protective role of the peritrophic matrix against intestinal bacterial infection in *Drosophila melanogaster*. *Proc Natl Acad Sci USA* **108**, 15966–15971.

Limmer S, Haller S, Drenkard E, Lee J, Yu S, Kocks C, Ausubel FM & Ferrandon D (2011). *Psedomonas aeruginosa* RhIR is required to neutralize the cellular immune response in a *Drosophila melanogaster* oral infection model. *Proc Natl Acad Sci USA* **108**, 17378–17383.

McDole JR, Wheeler LW, McDonald KG, Wang B, Konjufca V, Knoop KA, Newberry RD & Miller MJ (2012). Goblet cells deliver luminal antigen to CD103$^+$ dendritic cells in the small intestine. *Nature* **483**, 345–349.

Micchelli CA & Perrimon N (2006). Evidence that stem cells reside in the adult *Drosophila* midgut epithelium. *Nature* **439**, 475–479.

Molecular Devices (2011). Axopatch: determine the capacitance of my bilayer. Knowledgebase article 16628, http://mdc.custhelp.com/app/answers/detail/a_id/16628/kw/capacitance%20measurement

Naftalin RJ & Tripathi S (1986). The roles of paracellular and transcellular pathways and submucosal space in isotonic water absorption by rabbit ileum. *J Physiol* **370**, 409–432.

Ohlstein B & Spradling A (2006). The adult *Drosophila* posterior midgut is maintained by pluripotent stem cells. *Nature* **439**, 470–474.

Pal S, Lager RJS & Wu LP (2007). Fungal peptide Destruxin A plays a specific role in suppressing the innate immune response in *Drosophila melanogaster*. *J Biol Chem* **282**, 8969–8977.

Panayidou S & Apidianakis Y (2013). Regenerative inflammation: lesson from *Drosophila* intestinal epithelium in health and disease. *Pathogens* **2**, 209–231.

Rahat M & Dimentman CH (1982). Cultivation of bacteria-free *Hydra viridis*: missing budding factor in nonsymbiotic hydra. *Science* **216**, 67–68.

Robinson RA & Stokes RH (1970). *Electrolyte Solutions: The Measurement and Interpretation of Conductance, Chemical Potential and Diffusion in Solutions of Simple Electrolytes*, 2nd edn, ed. Robinson RA & Stokes RH. Butterworths Scientific Publications, London.

Ruiz-Sanchez E, Orchard I & Lange AB (2010). Effects of the cyclopeptide mycotoxin destruxin A on the Malpighian tubules of *Rhodnius prolixus* (Stål) *Toxicon* **55**, 1162–1170.

Ruiz-Sanchez E & O'Donnell MJ (2012). Effects of the microbial metabolite destruxin A on ion transport by the gut and renal epithelia of *Drosophila melanogaster*. *Arch Insect Biochem Physiol* **80**, 109–122.

Ryu J-H, Kim S-H, Lee H-Y, Bai JY, Nam Y-D, Bae J-W, Lee DG, Shin SC, Ha E-M & Lee W-J (2008). Innate immune homeostasis by the homeobox gene *Caudal* and commensal-gut mutualism in *Drosophila*. *Science* **319**, 777–782.

Sekirov I, Russel SL, Antunes LCM & Finlay BB (2010). Gut microbiota in health and disease. *Physiol Rev* **90**, 859–904.

Shanbhag S & Tripathi S (2005). Electrogenic H^+ transport and pH gradients generated by a V-H^+-ATPase in the isolated perfused larval *Drosophila* midgut. *J Membrane Biol* **206**, 61–72.

Shanbhag S & Tripathi S (2009). Epithelial ultrastructure and cellular mechanisms of acid and base transport in the *Drosophila* midgut. *J Exp Biol* **212**, 1731–1744.

Shanbhag S, D'Silva NM, Abraham TV & Tripathi S (2011). Electrolyte transport in the perfused *Drosophila* larval posterior midgut is selectively inhibited by paradoxical actions of fungal toxins. *Proc Physiol Soc* **24**, C14 and PC14.

Shanbhag S, Vazhappilly AT, Sane A, D'Silva NM, & Tripathi S (2013). Gut microbiota and the physiology of intercellular communication between larval enterocytes in *Drosophila*. 23rd European *Drosophila* Research Congress, Barcelona, P335.

Shen L, Weber CR, Raleigh DR, Yu D & Turner JR (2011). Tight junction pore and leak pathways: a dynamic duo. *Annu Rev Physiol* **73**, 283–309.

Taira J, Osada S, Hayashi R, Ueda T, Jelokhani-Niaraki M, Aoyagi H & Kodama H (2010). Trans-bilayer ion conductance by proline containing cyclic hexapeptides and effects of amino acid substitutions on ion conducting properties. *Bull Chem Soc Jpn* **83**, 683–688.

Tripathi S, Morgunov N & Boulpaep EL (1985). Submicron tip breakage and silanization control improve ion-selective microelectrodes. *Am J Physiol Cell Physiol* **249**, C514–C521.

Tripathi S & Hladky SB (1998). Streaming potentials in gramicidin channels measured with ion-selective microelectrodes. *Biophys J* **74**, 2912–2917.

Wang KW, Tripathi S & Hladky SB (1995). Ion binding constants for gramicidin A obtained from water permeability measurements. *J Membrane Biol* **143**, 247–257.

Weiss BL, Savage AF, Griffith BC, Wu Y & Aksoy S (2014). The peritrophic matrix mediates differential infection outcomes in the tsetse fly gut following challenge with commensal, pathogenic and parasitic microbes. *J Immunol* **193**, 773–782.

Wong, AC, Dobson AJ & Douglas AE (2014). Gut microbiota dictates the metabolic response of *Drosophila* to diet. *J Exp Biol* **217**, 1894–1901.

Wong AC, Luo Y, Jing X, Franzenburg S, Bost A & Douglas AE (2015). The host as the driver of the microbiota in the gut and external environment of *Drosophila melanogaster*. *Appl Environ Microbiol* **81**, 6232–6240.

Additional information

Competing interests

The authors declare no competing interests.

Author contributions

S.R.S. performed all microperfusion experiments and prepared the figures. T.V.A. performed all channel current recordings and set up all data acquisition instrumentation and software. A.S. performed the bilayer water permeability measurements. N.M.D. measured extracellular ion activity scans. S.T. designed the experiments. All authors were involved in data analysis, and participated in several rounds of manuscript writing and verification of data. The experiments were performed at the Tata Institute of Fundamental Research, Mumbai. All authors have approved the final version of the manuscript and agree to be accountable for all aspects of the work. All persons designated as authors qualify for authorship, and all those who qualify for authorship are listed.

Funding

This work was supported by Tata Institute of Fundamental Research Interdisciplinary Plan Programs 10P-809 and 11P-1606 to S.T.

Acknowledgements

We thank Mr Jyotish Parmar for unfailing help in high precision machining of microperfusion and electrophysiological apparatus. We thank Professor Raman Rajagopal and Dr N. Gayatri Priya, Gut Biology Laboratory, Department of Zoology, University of Delhi, for teaching us the preparation of sterile embryos. We thank Professors Emile Boulpaep and Clifford Slayman and Mr Victor Pantani at Yale University, Professor Barry Bowman at the University of California, Santa Cruz, and Professor Nilabh Shastri at the University of California, Berkeley, for discussions.

Authors' present addresses

A. Sane: Department of Bioengineering, University of Illinois at Chicago, 851 S. Morgan Street, Chicago, IL 60607-7052, USA.

N. M. D'Silva: Department of Biology, McMaster University, 1280 Main St. W., Hamilton, Ontario, Canada L8S 4K1.